# Segmentation of optic disc in retinal fundus images using fully convolutional network

*Sandip Sadhukhan[1], Goutam Kumar Ghorai[1], Debprasad Sinha[1], Souvik Maiti[1], Gautam Sarkar[1], Ashis Kumar Dhara[2]*

## Abstract

Background: Accurate segmentation of the Optic disc (OD) is important for computer-aided diagnosis of several ocular diseases such as glaucoma, diabetic retinopathy, and hypertensive retinopathy. This paper presents accurate and fast optic disc detection and segmentation method using U-Net based fully convolutional network. Sufficient number of annotated images is a bottleneck in medical image analysis and U-Net fills this gap by producing better segmentation results with a lower number of images. The network is trained from scratch using the fundus images of extended MESSIDOR database and the trained model is used for detection and segmentation of OD. The false positives are removed based on morphological operation and shape features. The result is evaluated using three-fold cross validation on six public fundus image databases such as DIARETDB0, DIARETDB1, DRIVE, AV-INSPIRE, CHASE DB1 and MESSIDOR. The U-Net based fully convolutional network is robust and effective for detection and segmentation of OD in the images affected by diabetic retinopathy and it outperforms existing techniques.

**Keywords**: Screening of ocular diseases, Retinal fundus image, Optic disc detection and segmentation, Fully convolutional network, and overlap measure

Visual impairment and blindness are a major problem of developing countries[1]. Diabetic retinopathy, hypertensive retinopathy, glaucoma are common causes of visual impairment and blindness[2]. Early diagnosis and appropriate referral for treatment of these diseases can prevent visual loss. Research is going on the development of computer-aided diagnosis system for accurate identification of different parts and pathologies in retinal fundus image to assist ophthalmologists. Optic disc is the entry point of the major blood vessels in the retina[3] and considered as landmark in retinal fundus image. Disc size and cup area are used for diagnosis of glaucoma[4,5]. The centre of optic disc is an important reference for detecting the macula and grading macular pathologies, such as diabetic maculopathy, macular edema, and macular ischemia[6]. Disc size is also an important parameter for determination of region of interest, where width of artery and vein need to be computed for diagnosis of hypertensive retinopathy[7]. Along with the position of the optic disc, the vessel origin is another important feature for vasculature analysis[8]. Automated detection and segmentation of the optic disc is a challenging problem due to the variation in size, shape, color, and the variation introduced by the field of view, inhomogeneous illumination, and pathological abnormalities. Shape and brightness[9,10,11] convergence of blood vessels[12,13] and orientation of blood vessels[13,14] have been investigated for detection of optic disc. The assumption of circular shape of optic disc does not hold good, where Optic Disc is partly present in the retinal image. Hoover et al.[12] resolved this issue poor contrast of optic disc by considering convergence of blood vessel in the optic disc.

Orientations of blood vessels have been used by Foracchia et al.[13] and Youssif et al.[14] to improve the result of Optic Disc localization. Vessel templates were also investigated by Osareh et al.[15] and Lowell et al.[3]. Active shape model is used to extract the main blood vessels for localization of OD[16]. Brightness characteristics of OD and vessel density in the OD region are utilized by Giachetti et al.[17]. Soares et al.[18] focused on the local appearance of the OD region and orientation of main blood vessels to determine the centre of OD. Vessel directional

[1]Electrical Engineering Department, Jadavpur University, India 700032, [2] Department of Electrical Engineering, National Institute of Technology, Durgapur, India-713209.
Corresponding Author: Sandip Sadhukhan, Email: sansad@gmail.com
Received on : 01/11/2019, Revision accepted on : 18/12/2019
Conflict of Interest : None, Financial Disclosure : None

and distribution of blood vessel is used by Zhang et al.[19] to improve accuracy of OD localization. Roychowdhury et al.[20] used region based features to classify the bright areas as OD and non-OD regions. The region with maximum vessel density and solidity is considered as the OD candidate.

The reported works on optic disc segmentation can be classified based on three categories - morphology, active contour model and active shape model. The OD boundary was segmented by Aquino et al.[8] by morphological operations, edge detection method and circular Hough transformation technique. Walter et al., Reza et al.[21], and Welfer et al.[22] determined the OD boundary using morphological operations and watershed transformation technique. Morales et al.[23] applied in painting as preprocessing for removing blood vessels and stochastic watershed transformation for determining the OD boundary. Caselles et al.[24] and Xu et al.[25] proved that segmentation can be performed better using active contour model (ACM). Snake-based ACM was used by Osareh et al.[15] to extract the OD boundary. In order to improve the accuracy of segmentation for low resolution images, Lowell et al.[3] applied a direction sensitive gradient-based technique to remove the vessel obstructions and deformable ACM for finding the OD boundary. Chrastek et al.[26] applied distance map algorithm to remove the blood vessels and then segmented the OD by using sequence of methods like morphological operation, Hough transformation and ACM. The method presented by Joshi et al.[4] improved the robustness of ACM proposed by Chan and Vese[27] by taking care of the variations in the OD region. Li and Chutatape[16] presented an active shape model based technique for OD segmentation.

Hybrid level set algorithm[28] was implemented by combining the local and regional gradient information of the fundus images. Morales et al.[23] detected the boundary of optic disc by the principal component analysis. Random forest[29,30] and boosting[31,32] have been used to predict the class probabilities of the pixels. These methods are prone to significant errors when certain geometric assumptions do not hold if precisely identification fails. Recently the ratio of people suffering from various kinds of eye diseases to that of available ophthalmologists particularly in developing countries is increasing in an alarming rate. An automated computer based system for analysis of fundus images would reduce the burden on the health care system of these kinds of countries. Advancement of deep learning based algorithms is playing an important role in designing such software systems. The success of convolutional neural network in object segmentation[33,34,35] has motivated us to investigate the performance of fully convolutional network for optic disc detection and segmentation. The major contributions of the present work are (i) initial segmentation of optic disc using U-Net based fully convolutional network and (ii) removal of false-positives based on anatomy-aware features.

In this paper, reported works on detection and segmentation of optic disc are reviewed in Introduction section. The proposed segmentation framework, experimental results and comparison of the proposed method with the state-of-the-art techniques is provided in the following sections.

## Material and Method:

### *Segmentation framework*

The proposed method (Fig.1) consists of initial segmentation using U-net[36] based fully convolutional network and reduction of false positives based on anatomy-aware features. The U-Net architecture is used for initial segmentation as it provides better segmentation using few numbers of training images.

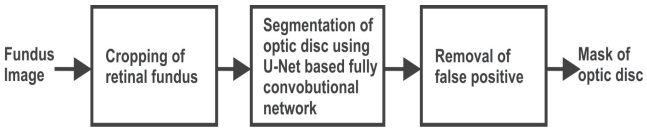


Fig.-1: Block diagram of the proposed segmentation framework

### *Preprocessing*

The images of different databases have different sizes. Therefore, the images are resized to 512 × 512 pixels for all databases. This process of resizing not only reduces the storage space of the database but also decreases the computational time without hampering the performance of the algorithm. The remaining operations are carried on these resized images. Red channel image is threshold. Morphological opening, closing and erosion operations with square structuring element are used to create a mask of circular retinal fundus region-of-interest, which allows focusing only on the foreground of retinal images. The fundus image is cropped based on the bounding box of this mask. The segmentation algorithm

is applied on cropped image to reduce the processing time.

## Segmentation using U-Net

### Architecture of U-Net

The U-net[36] is a fully convolutional network and the purpose of it is to use the high-level information and local appearance information of an object for improvement of segmentation. The network consists of a down-sampling path and an up-sampling path as shown in Fig. 2. The down-sampling path has 5 convolutional blocks and each block has two convolutional layers with a filter size of 3 × 3 and stride of 1. Max pooling with stride 2 is applied to the end of every blocks except the last block. U-Net learns weights in an end-to-end setting. The data is propagated through the network along all possible paths and generates the segmentation map at the end of the network. After each max pooling operation, the numbers of feature channels are doubled in the next convolution and ReLU level. The size of the input images is 512 × 512 and it decreases to 32 × 32 at the end of down-sampling path. The second part of the U-Net is the expansion layer which basically create the high resolution segmentation map.

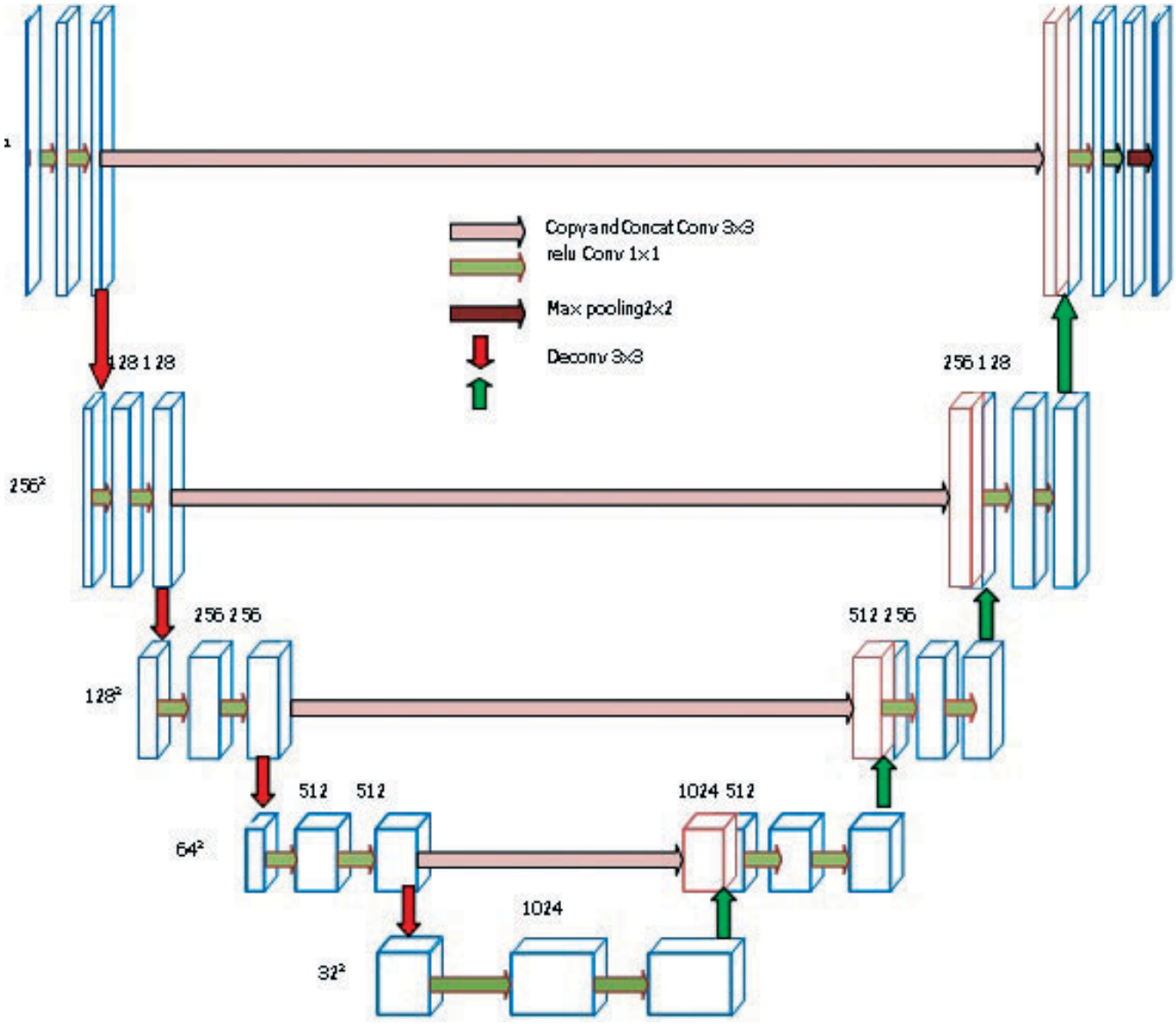


Fig.-2: Architecture of U-Net based fully convolutioal network.

This part consists of a sequence of up-convolutions and concatenation with high-resolution features from contraction path. Therefore, the size of feature maps increases from 32 × 32 to 512 × 512. High-level information is represented at up-sampling blocks, and low-level features are transferred through skip connection.

### *Training of U-Net*

The images of extended MESSIDOR database (MESSIDOR-II)[21] are used for training of U-Net from scratch. The database consists of total 1748 non-dilated macula-centered fundus images, captured by Topcon TRC NW6 non-mydriatic camera with a field-of-view of 45æ%. The fundus portion of the training images are cropped and then resized to a size of 512 × 512 pixels. Different augmentation (flip and rotation) is performed to improve the performance of U-net by large number of training images. A stochastic gradient-based optimization[37] (ADAM) is applied to minimize the cross-entropy based cost function. The cross-entropy loss function has been used for this purpose due to its efficiency in binary classification. ADAM utilizes the current gradients. The learning rate for the ADAM optimizer is set to 0.0001 and over-fitting is reduced by using dropout[31]. The weights of background and foreground are maintained as 1:10 and training were performed upto 60, 000 iterations. Fig. 3 presents the evolution of the loss on the training and validation data and proves that the trained network is not

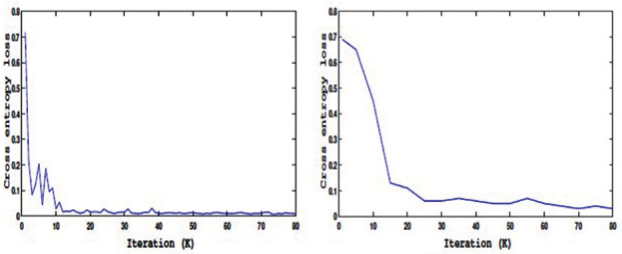


Fig.-3: (a) Training loss and (b) Validation loss with iterations.

over-fitted. The hyper-parameters are determined based on the validation dataset, which is 10% of the extended MESSIDOR database.

### *False positive removal*

Initial segmentation results may contain false positives caused by exudates as shown in Fig. 4(b) for the original image in 4(a). Morphological opening is applied to separate false positives from Optic disc. Generally, optic disc is circular or elliptical in nature. At first, compactness feature

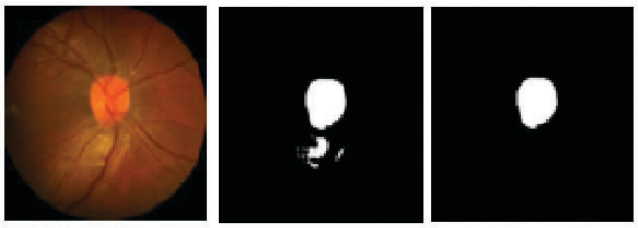

Fig.-4: (a) Original image (b) false positives caused by exudates (c) optic disc candidate.

is used to eliminate false positive candidates from initial segmentation results. Total number of candidates after this stage is two. The remaining false positive is eliminated by area of the object. The object having bigger size is considered as optic disc (Fig. 4(c)).

### *Database used for evaluation of segmentation result*

(a) Messidor: MESSIDOR[38] database contains 1200 colour retinal images, acquired using non-mydriatic camera. Binary mask of the optic disc of MESSIDOR dataset was provided by the experts of the University of Huelva.

(b) DIARETDB0: This database[39] consists of 130 color fundus images [1500 x1152 pixels] for diabetic retinopathy detection benchmarking exercise. Out of this total set, 110 images contain signs of the diabetic retinopathy which includes hard exudates, soft exudates, micro-naneuyrysms, hemorrhages and neovascularization.

(c) DIARETDB1: It consists[40] of 89 colour fundus images [1500 x 1152 pixels] of mixed nature - 5 are normal images and 84 images are having some mild non-proliferative signs of the diabetic retinopathy. In this dataset, the abnormalities are relatively smaller and found near macula.

(d) DRIVE: This database[41] consists of total 40 images [565 x 584 pixels] which help comparative studies on blood vessels segmentation. These were obtained during a diabetic retinopathy screening program on an age group of 25-90 years in The Netherlands.

(e) AV-INSPIRE: This database is based on the INSPIRE-AVR dataset[42], which is having 40 images [2392 X 2048 pixels]. The main purpose of this set is to estimate and compare the arteriolar-venular ratio.

(f) CHASE DB1: This database[23] consists of total 28 paired images [999 X 960 pixels] captured from 14 children as part of the Child Heart and Health Study in England

(CHASE). The images of this set are of poor contrast quality as well as affected by illumination artefacts

### Evaluation

The performance of optic disc detection is evaluated using success rate (SR) and it represents the percentage of retinal images in a dataset where the centroid of optic disc is successfully localized within the boundary of the ground truth mask of optic disc. The performance of optic disc segmentation is evaluated in terms of a region based metric Overlap Measure (OM) and a contour-based metric mean absolute distance (MAD)[20].

The OM represents the ratio of the intersecting area between the actual optic disc and segmented optic disc and it is defined as

$$OM = \frac{N_{tp}}{N_{tp} + N_{fp} + N_{fn}} \qquad (1)$$

where $N_{tp}$, $N_{fp}$ and $N_{fn}$ are number of true positive, false positive and false negative pixels respectively.

MAD represents the mean of the shortest distances from the boundary of the actual optic disc to the boundary of the segmented optic disc. Let $P_{i'}$, where i'= 1, . . ., $m_C$ and $Q_{j'}$, where, j' = 1,. . ., $n_{\hat{C}}$ are the boundary points obtained on the segmented and actual optic disc boundaries respectively. The shortest distance from each boundary point of the segmented optic disc to the boundary points on the boundary points of ground truth mask of optic disc is calculated using Equation-2 and the shortest distance from each boundary point of the ground truth mask optic disc to the boundary points on the boundary points of segmented optic disc is calculated using Equation-3. Mean of the obtained shortest distances is calculated using Equation 4.

$$m_{C,\hat{C}}(i') = \min \left\| P_{i'} - Q_{j'} \right\|_2 \qquad (2)$$

$$m_{\hat{C},C}(i') = \min \left\| Q_{j'} - P_{i'} \right\|_2 \qquad (3)$$

$$MAD = \frac{1}{2}\left\{ \frac{1}{n_c} \sum_{i'}^{m_c} m_{C,\hat{C}}(i) + \frac{1}{n_{\hat{C}}} \sum_{j'}^{n_{\hat{C}}} m_{\hat{C},C}(j) \right\} \qquad (4)$$

## Result:

### Quantitative analysis

The evaluation of the proposed segmentation algorithm was performed on DIARETDB0, DIARETDB1, DRIVE, AV-INSPIRE, CHASE DB1 and MESSIDOR datasets. For each of the dataset, we divided the images into three subsets, of which, two are used for fine tuning of the pre-trained network and remaining set is used for testing. Thus U-Net learns database specific features through the transfer learning. The average value of SR, OM, and MAD of the proposed framework and competing techniques are provided in Table-1 for six public fundus image database. The OM of the proposed method is larger as compared to the competing techniques. Such improvement of OM is due to the application of fully convolutional network in initial segmentation.

A comparison of segmentation performance in terms of percentage of test images included in various OM distributions, is provided in Table-2.

### Qualitative results

This methodology needs to be stable in databases consisting of dilated and non-dilated fundus images. We have analysed the proposed framework for images of healthy subjects [Fig. 5(a)-(f)], the images with the presence of pathologies [Fig. 6(a)-(f)], and low contrast

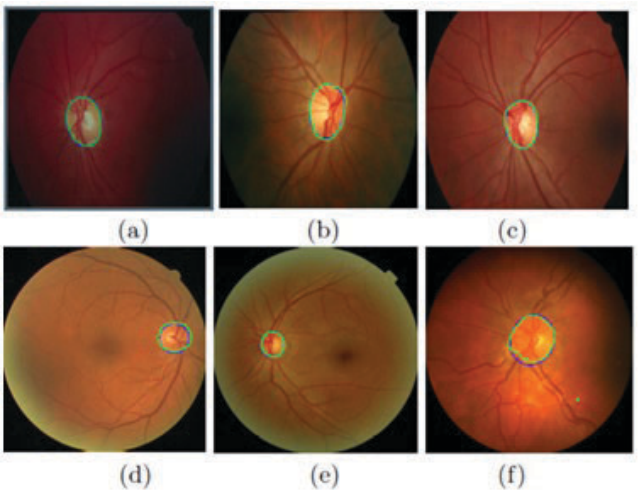


Fig.-5: Segmentation evaluation examples for normal fundus images. Sample images are from (a)-(c)- DIARETDB0; (d)- DRIVE; (e)- MESSIDOR; (f)-CHASE dataset. The contour of ground truth and segmented optic disc is shown in blue and green color respectively.

Table-1: Comparative result of optic disc segmentation

| Method | Author | OM | MAD | SR |
|---|---|---|---|---|
| DIARETDB1 | **Proposed** | **0.91** | **2.22** | **100** |
| | Roychowdhury *et al.*[20] | 0.80 | 4.82 | 100 |
| | Morales et al.[23] | 0.82 | 2.88 | 100 |
| | Salazar et al.[43] | 0.76 | 6.38 | 96.7 |
| | Welfer et al.[22] | 0.43 | 8.31 | 97.7 |
| DIARETDB0 | **Proposed** | **0.81** | **4.76** | **97.75** |
| | Roychowdhury et al. [20] | 0.78 | 4.91 | - |
| DRIVE | **Proposed** | **0.86** | **2.63** | **97.5** |
| | Roychowdhury et al. [20] | 0.81 | 5.01 | 100 |
| | Morales et al[23] | 0.72 | 5.85 | 100 |
| | Salazar et al.[43] | 0.71 | 6.68 | 97.5 |
| | Welfer et al.[22] | 0.42 | 5.74 | 100 |
| MESSIDOR | **Proposed** | **0.91** | **1.97** | **99.92** |
| | Roychowdhury et al.[20] | 0.84 | 3.9 | 100 |
| | Marin et al.[44] | 0.87 | 6.17 | 99.75 |
| | Giachetti et al.[17] | 0.88 | - | 99.83 |
| | Aquino et al.[8] | 0.86 | - | 98.83 |
| | Yu et al.[45] | 0.83 | 7.7 | 99.08 |
| CHASE DB1 | **Proposed** | **0.81** | **7.55** | **100** |
| | Roychowdhury et al.[20] | 0.81 | 5.19 | - |
| AV INSPIRE | **Proposed** | **0.82** | **4.90** | **100** |

Table-2: Percentage of images in various OM levels

| Method | Author | OM ≥ 0.7 | OM ≥ 0.75 | OM ≥ 0.85 | OM ≥ 0.9 |
|---|---|---|---|---|---|
| DIARETDB1 | **Proposed** | **90.80** | **86.21** | **45.98** | **17.24** |
| | Roychowdhury *et al.* [20] | 91.13 | 73.41 | 32.91 | 10.12 |
| | Salazar *et al.*[43] | 70.78 | 60.67 | 32.58 | 11.24 |
| | Boykov *et al.*[46] | 38.2 | 28.09 | 8.99 | 2.25 |
| | Zeng *et al.* [47] | 10.11 | 5.62 | 2.25 | 1.12 |
| DIARETDB0 | **Proposed** | **96.36** | **96.36** | **90.91** | **80.91** |
| | Roychowdhury *et al.* [20] | 82.5 | 68.34 | 26.67 | 4.16 |
| DRIVE | **Proposed** | **97.44** | **97.44** | **74.46** | **30.77** |
| | Roychowdhury *et al.* [20] | 93.3 | 83.3 | 40 | 16.7 |
| | Salazar *et al.* [43] | 57.5 | 50 | 25 | 5 |
| | Boykov *et al.*[46] | 27.5 | 12.5 | 0 | 0 |
| | Zeng *et al.* [47] | 20 | 17.5 | 7.5 | 2.5 |
| MESSIDOR | **Proposed** | **98.00** | **97.08** | **90.91** | **76.98** |
| | Roychowdhury *et al.* [20] | 96.72 | 82.85 | 47.56 | 20 |
| | Marin *et al.*[44] | 95 | - | 83.75 | 48.92 |
| | Giachetti *et al.* [44] | 92-94 | 89-92 | 78-82 | 59-62 |
| | Yu *et al.*[45] | 77 | 77 | 45 | 25 |
| | Aquino *et al.*[8] | 93 | 90 | 73 | 46 |
| CHASE DB1 | **Proposed** | **85.71** | **82.14** | **67.86** | **39.39** |
| | Roychowdhury *et al.*[20] | 89 | 83.33 | 44.44 | 11.11 |
| AV INSPIRE | **Proposed** | **92.50** | **80.00** | **60.00** | **22.50** |

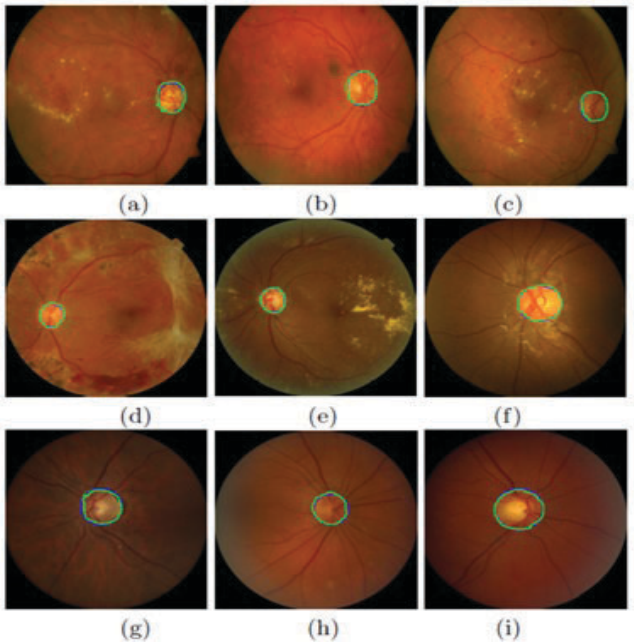


Fig.-6: Segmentation evaluation examples for images having pathologies and haemorrhage (a)-(f), low contrast (g)-(i). Sample images are from (a)-(c)- DIARETDB1; (d),(e)- MESSIDOR;(f)-CHASE; (g)-(i)-INSPIRE dataset. The contour of ground truth and segmented optic disc is shown in blue and green color respectively.

[Fig. 6(g)-(i)]. These qualitative results reveal that the proposed algorithm is capable of identifying the optic disc in bad quality retinal images also. Few images with poor segmentation results is shown in [Fig. 7(a)-(c)]. The poor segmentation is due to non-uniform illumination due to image acquisition.

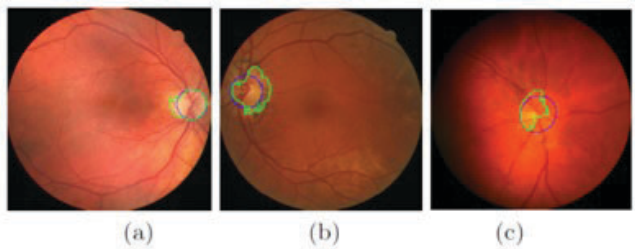


Fig.-7: Segmentation evaluation examples for failed cases. Sample images are from (a),(b)-DRIVE; (c)-CHASE dataset. The contour of ground truth and segmented optic disc is shown in blue and green color respectively.

### *Implementation*

The U-Net architecture is implemented in Python using the PyTorch library in in Linux environment using a 8 GB GPU (NVIDIA GeForce GTX 1070 with 8GB GDDR5 memory) on a system with Core-i7 processor and 32 GB RAM.

## Discussion:

In case of DIARETDB1, CHASE DB1, and AV INSPIRE optic disc are successfully detected for all images. The numbers of failure cases for optic disc detection are 2, 1 and 1 for DIARETDB0, DRIVE, and MESSIDOR, respectively. The MAD values of the proposed method are slightly better or comparable with the competing techniques for different database. The high value of OM depict that the segmented mask of optic disc matches accurately with the ground truth mask. The proposed method outperforms the competing techniques at three different OM levels such as e" 0.75, 0.85 and 0.9. The proposed method also performs better for DIARETDB0, DRIVE, MESSIDOR dataset at OM e"0.7.

In the proposed method, fully convolutional network is trained by feeding thousands of varying grades of fundus images, where it is learns the best features on its own. Therefore, the proposed method outperforms the other competing techniques in most of the metrics measurements. The method is also successful in optic disc localization and segmentation, when tested on both dilated and non-dilated types of fundus images acquired from different medical centres. The performance of this algorithm does not degrade while handling images containing strong distractors like yellowish exudates which prove the effectiveness and robustness of the proposed process. In future more research needs to be accomplished to increase the accuracy of the optic disc segmentation with much larger volume of retinal images.

## References:

1. Bourne RR, Flaxman SR, Braithwaite T, et al.: Magnitude, temporal trends, and projections of the global prevalence of blindness and distance and near vision impairment: a systematic review and meta-analysis. The Lancet Global Health. 2017;5:e888–e97
2. Pascolini D, Mariotti S. Global estimates of visual impairment: 2010. British Journal of Ophthalmology. 2012;96:614–8.
3. Lowell J, Hunter A, Steel D, et al. Optic nerve head segmentation. IEEE Transactions on medical Imaging. 2004;23: 256–64.
4. Joshi GD, Sivaswamy J, Krishnadas S. Optic disk and cup segmentation from monocular color retinal images for glaucoma assessment. IEEE transactions on medical imaging. 2011;30:1192–205.
5. Cheng J, Liu J, Xu Y, et al. Superpixel classification based optic disc and optic cup segmentation for glaucoma screening. IEEE Transactions on Medical Imaging. 2013;32:1019–32.

6. Qureshi RJ, Kovacs L, Harangi B, et al. Combining algorithms for automatic detection of optic disc and macula in fundus images. Computer Vision and Image Understanding. 2012;116:138–45.
7. Estrada R, Tomasi C, Schmidler SC, Farsiu S. Tree topology estimation. IEEE transactions on pattern analysis and machine intelligence. 2015;37:1688–701.
8. Aquino A, Gegu´ndez-Arias ME, Mar´ýn D. Detecting the optic disc boundary in digital fundus images using morphological, edge detection, and feature extraction techniques. IEEE transactions on medical imaging. 2010;29:1860–9.
9. Barrett S, Naess E, Molvik T. Employing the hough transform to locate the optic disk. Biomedical sciences instrumentation. 2001;37:81–6.
10. Sinthanayothin C, Boyce JF, Cook HL, Williamson TH. Automated localisation of the optic disc, fovea, and retinal blood vessels from digital colour fundus images. British Journal of Ophthalmology. 1999;83: 902–10.
11. Blanco M, Penedo MG, Barreira N, et al. Localization and extraction of the optic disc using the fuzzy circular hough transform. In: International Conference on Artificial Intelligence and Soft Computing. Springer 2006;712–21.
12. Hoover A, Goldbaum M. Locating the optic nerve in a retinal image using the fuzzy convergence of the blood vessels. IEEE transactions on medical imaging. 2003;22:951–8.
13. Foracchia M, Grisan E, Ruggeri A. Detection of optic disc in retinal images by means of a geometrical model of vessel structure. IEEE transactions on medical imaging. 2004;23:1189–95.
14. Youssif AAHAR, Ghalwash AZ, Ghoneim AASAR. Optic disc detection from normalized digital fundus images by means of a vessels' direction matched filter. IEEE Transactions on Medical imaging. 2008;27:11–8.
15. Osareh A, Mirmehdi M, Thomas B, Markham R. Comparison of colour spaces for optic disc localisation in retinal images. In: Pattern Recognition, 2002. Proceedings. 16th International Conference on, IEEE 2002;vol.1:743–6.
16. Li H, Chutatape O. Automated feature extraction in color retinal images by a model based approach. IEEE Transactions on biomedical engineering. 2004;51:246–54.
17. Giachetti A, Ballerini L, Trucco E. Accurate and reliable segmentation of the optic disc in digital fundus images. Journal of Medical Imaging. 2014;1:024,001–024,001.
18. Soares I, Castelo-Branco M, Pinheiro A.M. Optic disc localization in retinal images based on cumulative sum fields. IEEE journal of biomedical and health informatics. 2016;20:574–85.
19. Zhang D, Zhao Y. Novel accurate and fast optic disc detection in retinal images with vessel distribution and directional characteristics. IEEE journal of biomedical and health informatics 2016;20:333–42.
20. Roychowdhury S., Koozekanani DD, Kuchinka SN, Parhi KK. Optic disc boundary and vessel origin segmentation of fundus images. IEEE journal of biomedical and health informatics 2016;20:1562–74.
21. Reza AW, Eswaran C, Hati S. Automatic tracing of optic disc and exudates from color fundus images using fixed and variable thresholds. Journal of medical systems 2009;33:73.
22. Welfer D, Scharcanski J, Kitamura CM, et al. Segmentation of the optic disk in color eye fundus images using an adaptive morphological approach. Computers in Biology and Medicine 2010;40:124–37.
23. Morales S, Naranjo V, Angulo J, Alcan˜iz M. Automatic detection of optic disc based on pca and mathematical morphology. IEEE transactions on medical imaging 2013;32:786–96.
24. Caselles V, Kimmel R, Sapiro G. Geodesic active contours. International journal of computer vision 1997;22:61–79.
25. Xu C, Prince JL. Snakes, shapes, and gradient vector flow. IEEE Transactions on image processing 1998;7:359–69.
26. Chrstek R, Wolf M, Donath K, et al. Automated segmentation of the optic nerve head for diagnosis of glaucoma. Medical Image Analysis 2005;9:297–314.
27. Chan TF, Vese LA. Active contours without edges. IEEE Transactions on image processing 2001;10:266–77.
28. Zhang Y, Matuszewski BJ, Shark LK, Moore CJ. Medical image segmentation using new hybrid level-set method. In: BioMedical Visualization, 2008. MEDIVIS'08. Fifth International Conference, IEEE 2008;71–6.
29. He X, Zemel RS, Carreira-Perpin˜´an MA´. Multiscale conditional random fields for image labeling. In: Computer vision and pattern recognition, 2004. CVPR

2004. Proceedings of the 2004 IEEE computer society conference on, IEEE 2004;vol.2:II–II.

30. Russell C, Kohli P, Torr PH, et al. Associative hierarchical crfs for object class image segmentation. In: Computer Vision, 2009 IEEE 12th International Conference on, IEEE 2009;739–46.
31. Lempitsky V, Vedaldi A, Zisserman A. Pylon model for semantic segmentation. In: Advances in neural information processing systems, 2011;1485–93.
32. Delong A, Osokin A, Isack HN, Boykov Y. Fast approximate energy minimization with label costs. International journal of computer vision 2012;96:1–27.
33. Papandreou G, Kokkinos I, Savalle PA. Modeling local and global deformations in deep learning: Epitomic convolution, multiple instance learning, and sliding window detection. In: Computer Vision and Pattern Recognition (CVPR), 2015 IEEE Conference on, IEEE 2015;390–99.
34. Chen X, Mottaghi R, Liu X, et al. Detect what you can: Detecting and representing objects using holistic models and body parts. In: Proceedings of the IEEE Conference on Computer Vision and Pattern Recognition, 2914;1971–8.
35. Cordts M, Omran M, Ramos S, et al. The cityscapes dataset for semantic urban scene understanding. In: Proceedings of the IEEE conference on computer vision and pattern recognition, 2016;3213–23.
36. Ronneberger O, Fischer P, Brox T. U-net: Convolutional networks for biomedical image segmentation. In: International Conference on Medical Image Computing and Computer- Assisted Intervention, Springer 2015;234–41.
37. MESSIDOR-2: Messidor-2. digital retinal images, latim laboratory (http://latim.univ-brest.fr/), and the messidor program partners 2010 (http://messidor.crihan.fr/).
38. MESSIDOR: Messidor. digital retinal images, messidor techno-vision project, france. 2014; http://messidor.crihan.fr/download-en.php (download images section).
39. Kauppi T, Kalesnykiene V, Kamarainen JK, et al. Diaretdb0: Evaluation database and methodology for diabetic retinopathy algorithms. Machine Vision and Pattern Recognition Research Group, Lappeenranta University of Technology, Finland 2006;73.
40. K¨alvi¨ainen R, Uusitalo H. Diaretdb1 diabetic retinopathy database and evaluation protocol. In: Medical Image Understanding and Analysis, Citeseer 2007;2007:61.
41. Staal J, Abr'amoff MD, Niemeijer M, et al. Ridge-based vessel segmentation in color images of the retina. IEEE transactions on medical imaging 2004;23:501–9.
42. Niemeijer M, Xu X, Dumitrescu A, et al. Inspire-avr: Iowa normative set for processing images of the retina-artery vein ratio 2011.
43. Salazar-Gonzalez AG, Li Y, Liu X. Optic disc segmentation by incorporating blood vessel compensation. In: Computational Intelligence In Medical Imaging (CIMI), 2011 IEEE Third International Workshop On, IEEE 2011;1–8.
44. Marin D, Gegundez-Arias ME, Suero A, Bravo JM. Obtaining optic disc center and pixel region by automatic thresholding methods on morphologically processed fundus images. Computer methods and programs in biomedicine 2015;118:173–85.
45. Yu H, Barriga ES, Agurto C, et al. Fast localization and segmentation of optic disk in retinal images using directional matched filtering and level sets. IEEE Transactions on information technology in biomedicine 2012;16:644–57.
46. Boykov Y, Funka-Lea G. Graph cuts and efficient nd image segmentation. International journal of computer vision 2006;70:109-31.
47. Zeng Y, Samaras D, Chen W, Peng Q. Topology cuts: A novel min-cut/max-walgorithm for topology preserving segmentation in n{d images. Computer vision and image understanding 2008;112:81-90.

Cite this article as:
Sadhukhan S, Ghorai GK, Sinha D, Maiti S, Sarkar G, Dhara AK. Segmentation of optic disc in retinal fundus images using fully convolutional network. Current Indian Eye Research 2019;6:40-48.